University of Crete

Department of Biology

Master Thesis
in Protein Biotechnology

Design of functionalized surfaces for acoustic studies of biomolecules

Papagavriil Fotini

Supervised by
Prof. Electra Gizeli

Heraklion, October 2018

University of Crete
Department of Biology

First of all I would like to acknowledge Prof. Electra Gizeli from the Biosensors Lab. for her guidance and for giving me the opportunity to do my master thesis in her laboratory.

Special thanks to Dr. Pablo Mateos-Gil and Dr. Achilleas Tsortos for supervising my work.

Protein constructs were kindly provided by Marino Zerial's Lab at the Max Planck Institute of Molecular Cell biology & Genetics, Dresden, Germany.

Abstract

Acoustic biosensors are analytical devices that use ultrasound waves to extract information about a molecule of interest. More specifically, Quartz Crystal Microbalance with Dissipation monitoring (QCM-D) has been used to follow interactions between attached molecules and solid surfaces. Thus QCM-D has been able to probe viscoelastic properties of films formed by biomolecules at the interface between solid surfaces and liquid. In order to monitor these reactions the surface chemistry must be carefully designed.

For the quantitative and qualitative interpretation of QCM-D data, we used a discrete-molecule binding theory combined with designed surfaces to follow molecular hydrodynamic properties of molecules. The model suggests that the acoustic ratio $\Delta D/\Delta f$ is related to the intrinsic viscosity $[\eta]$, a measure of the hydrodynamic properties of bound biomolecules.

Two different surfaces were used in order to immobilize (a) DNA molecules of various lengths and (b) C terminal constructs of a coiled-coil protein involved in endosomal trafficking. In both cases, Supported Lipid Bilayers (SLB) were first formed, following the binding of discrete molecules that maintain their native structure.

For the immobilization of DNA molecules we used the biotin-streptavidin interaction that has been widely exploited for nucleic acid detection using QCM-D monitoring. In previous work biotinylated DNA molecules were immobilized at surfaces covered with neutravidin. In this report we try to elucidate the "linker effect" to evaluate the effect of different linking strategies between the sensor surface and DNA molecules. For this reason we tested the biotin-streptavidin system on Supported Lipid Bilayers (SLBs). The results suggest that the "linker" between sensor surface and target DNA, affects significantly the acoustic measurements.

For the specific immobilization of Early endosomal antigen 1 (EEA1) constructs, SLBs containing Phosphatidylinositol 3-phosphate (PI3P) lipids were prepared. In order to apply the discrete molecule approach we used different protein concentration on those surfaces. This particular SLB lipid composition allowed the stable immobilization of protein constructs and preliminary acoustic measurements were evaluated.

Contents

List of Figures

1 Introduction

1.1 Acoustic Biosensors- Theory and Background

Acoustic wave biosensors are analytical devices capable to detect a wide range of biological analytes such as DNA,RNA and proteins and the interactions between them. Different kind of information can be extracted from these devices. In particular, inherent characteristics of the adsorbed molecules (e.g. their mass, viscoelastic properties, size and shape) can be obtained by following the properties of acoustic waves that are generated at the surface of the sensor (i.e. frequency, amplitude).
There are two main types of acoustic wave devices: bulk acoustic wave sensors (BAW) and surface acoustic wave sensors (SAW). SAW and BAW devises work in similar ways. They use piezoelectric materials to generate and detect acoustic waves. These waves are either standing (BAW sensor, fig. 1.1a) or propagate parallel to the surface of the piezoelectric substrate (SAW sensor, fig. 1.1b).

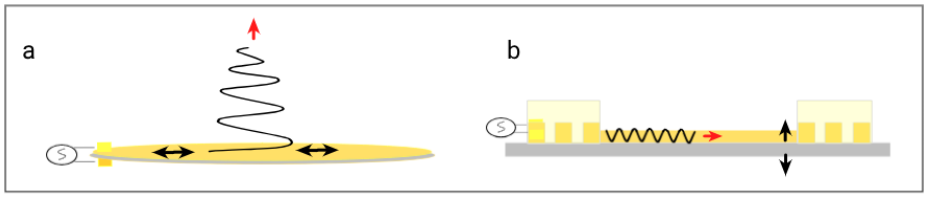

Figure 1.1: Schematic representation of characteristic BAW (a) and SAW (b) devices. In BAW devices, voltage is applied to the electrodes sandwiching the piezoelectric crystal. This is causing a "shear motion" (black arrows) and the acoustic wave penetrates into the bulk perpendicular to the surface. In SAW devices the wave propagation is in parallel with substrate.

In this study we use bulk acoustic wave sensors. In particular Quartz Crystal Microbalance with Dissipation monitoring (QCM-D) to monitor the binding of DNA and protein molecules on different surfaces.

1.1.1 Quartz Crystal Microbalance with Dissipation monitoring (QCM-D)

QCM-D is based on the converse piezoelectric effect, where application of voltage across the surface of various crystals (e.g. quartz, zinc oxide, gallium arsenide) afford a corresponding mechanical deformation. The QCM sensor is a thin AT-cut quartz crystal sandwiched between two electrodes. When applying AC the crystal oscillates in a thickness-shear mode (TSM) where the two surfaces move in an anti-parallel way.

The are two main ways to obtain information about the standing waves that are generated in the crystal. First, the 'impedance analysis' method where the whole resonant peak is

recorded and two parameters are obtained: the resonance frequency (f) and the bandwidth Γ (fig 1.2, upper panel).

The second way is referred to the "ring-down" method which is used in QCM-D. In this case the driving voltage, producing the acoustic wave, is switched off [2] and the crystal oscillations are left to decay (fig. 1.2, bottom panel). The signal of the decaying mechanical oscillations is recorded, giving two parameters, the resonance frequency (f) and the energy dissipation (D) (Fig.1.2).

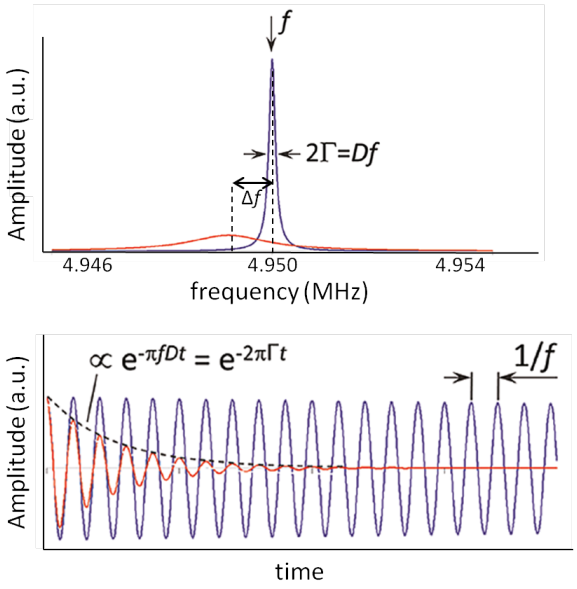

Figure 1.2: Resonance observed when crystal is in air (blue) and liquid (red). Two parameters are used to characterize the resonance: frequency f and bandwidth Γ. In QCM-D, the resonance frequency f and energy dissipation D are extracted from the decay curve. Figure adapted from [3].

Historically the use of quartz crystals as microbalances is based on the Sauerbrey equation which established the proportionality between the shift in resonance frequency and the adsorbed mass on the QCM sensor:

$$\Delta \mathrm{m} = \frac{C}{n} \Delta \mathrm{f} \ , \ \mathrm{n}=1,3,5,7$$

where n is the harmonic and C is the mass sensitivity constant which depends on the fundamental frequency and the material properties of the quartz crystal (density and thickness etc.). For a 5 MHz crystal, C = $\sim 17.7 \mathrm{ng/cm}^2\ Hz^{-1}$.

In order for the Sauerbrey relation to hold, there are some conditions that must be fulfilled. The adsorbed mass must be very small (relative to the mass of the crystal) and evenly distributed in the surface of the crystal. More importantly this mass must be rigidly adsorbed so that it oscillates in phase with the shear oscillation of the quartz. As an example of Sauerbrey equation applicability, QCM has been used for measuring the thickness of metal films deposition. In contrast when used to study soft viscoelastic films, these films do not follow the sensor's oscillation, thus the frequency of the oscillation is not influenced only by

the mass of the film. This issue has been solved by measuring the damping (energy dissipation) of the sensor, giving a quantitative measure of the losses induced by a viscoelastic material. The dissipation factor is defined as the inverse of Q factor:

$$D = \frac{1}{Q} = \frac{E_{dissipated}}{2\pi\ E_{stored}}$$

where $E_{dissipated}$ is the energy dissipated during one oscillation cycle and E_{stored} is the energy stored in the system.
When soft films are deposited on the surface of the sensor the rate of decay is much faster compared to solid films as shown in Fig. 1.3.

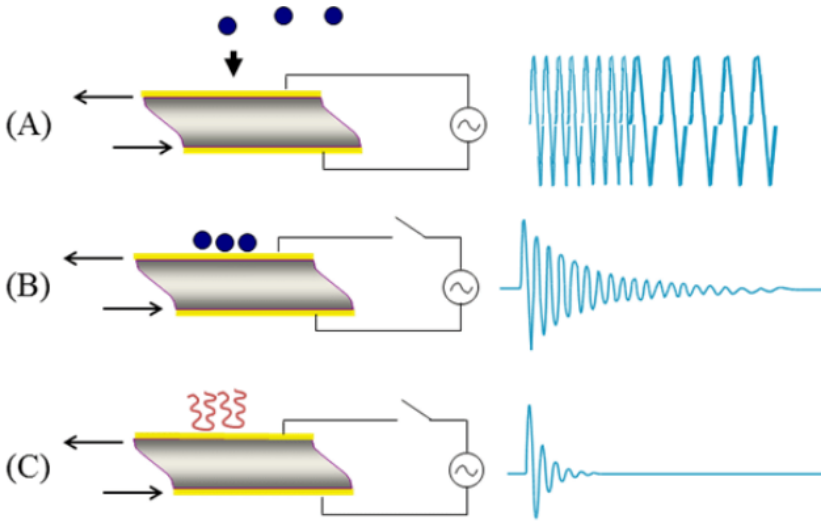

Figure 1.3: Schematic illustration of crystal oscillation. Mass is attached to the surface causing a decrease in frequency (A). Driving voltage is switched off and the crystal oscillation decay is monitored for rigid (B) and soft (C) molecules. Figure adapted from [4].

1.1.2 Data Modelling and Interpretation

Films can be classified in different types: homogeneous or heterogeneous and continuous or discrete. As mentioned previously the Sauerbrey model can be applied with certain restrictions. As soon as there is a viscoelastic behavior (dissipation factor is not zero) in an adsorbed film, the mass is not fully coupled to the motion of the sensor and thus Δf does not respond only to Δm. There are different approaches used for the modelling and interpretation of QCM-D data. Besides the Sauerbrey model, several other models are used depending on the material properties of the adsorbed layer. For example the Maxwell model which is usually used for polymer solutions that resemble liquid materials or the Voight model for more viscoelastic materials [5].

Continuous-homogeneous films

QCM data for homogeneous films are usually analyzed using continuous models such as Voight and Sauerbrey model. The fitting of Voight model to experimental data of multiple

overtones gives the thickness, density and rigidity modulus of the adsorbed layer. As mentioned in the previous section, the films that are formed can either induce small or great dissipative losses. In practice, for easier and more accurate distinction between these films, the acoustic ratio between the change in energy dissipated and the change in frequency, $\Delta D/\Delta f$, can be taken into account. For a value of $\Delta D/\Delta f \sim 0.4 * 10^{-6} * Hz^{-1}$ or below, the film can be considered as rigid, thus the Sauerbrey equation can be used to obtain mass of the layer [3]. The Voight model is used with certain assumptions. The thickness, t_f, and density, ρ_f, of the film are uniform. At the same time the viscoelastic properties of shear modulus and viscosity are not dependent on the frequency, and that there is no slip between the adsorbed layer and the crystal during the oscillations (Fig 1.4).

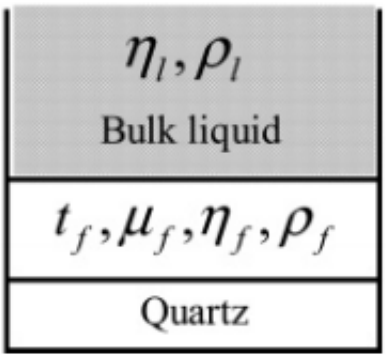

Figure 1.4: QCM sensor covered by a film with a thickness, t_f, shear modulus, μ_f, shear viscosity, η_f and density, ρ_f in contact with liquid [1].

There are several reports that compare the Sauerbrey and the Voight model in order to elucidate in what range those models apply [1, 6]. In particular, Cho et al. [1] tested the validity of the Sauerbrey relation for soft and rigid films by calculating the layer thickness. They followed the rupture of lipid vesicles and compared the results with calculations from the Voight model. Due to the highly viscoelastic character of intact vesicles the Sauerbrey equation underestimated the thickness of the layers. After the vesicle rupture the layer thickness agreed for both models. In another example [6], protein molecules were adsorbed onto a surface, inducing a large dissipation change ($\Delta D \sim 16 * 10^{-6}$). This value indicates that the resulting protein layer is highly viscoelastic. After adding a cross-linking molecule the dissipation factor decreases to almost zero indicating the formation of a more rigid layer. By following the changes in D, the group was able to monitor the structural transformation of the film and compared their results with data using both the Sauerbrey and Voight model and ellipsometry as an independent measurement.

Discrete particle approach

The previously described models derive information (thickness, rigidity) related to uniform films of molecules. However, many of these molecules do not necessarily form films. The conservation of their native structure is of great importance as it directly impacts their functionality. Modelling and molecular simulations play a significant role in order to obtain information about molecules as surface-bound isolated entities instead of films. Finite element method (FEM) [7, 8] and other simulations [9] have been used to derive the theoretical frequency and dissipation changes of acoustic waves. The frequency shift is proportional to the lateral stress applied by the molecule onto the crystal surface. This stress can be modelled to obtain the distribution of pressure and dissipated energy inside and around the sample as well. In an alternative approach, in the work of Tsortos et al [10, 11], the acoustic ratio between the energy dissipation and the frequency change ($\Delta D/-\Delta f$) is correlated to the intrinsic viscosity $[\eta]$ of the surface-bound biomolecules. These works demonstrate

the hydrodynamic nature of interaction between acoustic waves and biomolecules. Intrinsic viscosity is a characteristic of the shape and size of a biomolecule. This information was able to distinguish between different shapes and sizes of a range of DNA molecules[12]. The approach has been proven true for protein molecules as well [13, 14] (discussed in next section).

1.1.3 QCM-D Applications

The QCM-D technology has been widely used for studies of biological interest since it offers the possibility to work in liquid and it can monitor changes of the acoustic waves in real time without the requirement of labels. It has been used to measure DNA and RNA hybridization [15, 16], protein and cell adsorption onto surfaces [17, 18, 19], antibody-antigen [20, 21] interactions and formation of lipid bilayers [22, 23, 24]. Considering its sensitivity for mass detection and ability to track the formation and the changing structure of functional biomolecules, there is great interest on using this technique to extract conformational information (size, shape, orientation) of molecules attached on surfaces.

DNA

QCM has been widely applied in studies of DNA adsorption onto different surfaces, DNA hybridization, drug and gene delivery [25, 26, 27] and DNA-protein interactions [28]. A common strategy for developing biosensor/biochips to couple DNA molecules involves Self-Assembled Monolayers (SAMs). Although gold surfaces modified with thiolated DNA proved to be greatly heterogeneous, modifications of the adsorption method resulted in surfaces with fewer aggregates and lower DNA surface concentration [29]. QCM combined with fluorescence microscopy has been also used to characterize the immobilization and hybridization of thiol-modified DNA oligomers (single or double stranded) on Au surfaces in response to different buffer, salt concentration and temperature [15]. An alternative way to follow hybridization process is by monitoring the structural evolution of the DNA strands during the reaction [16]. This approach is based on the binding of discrete molecules rather than the formation of films.

Efficiency and reproducibility of hybridization is of great importance for DNA functionalized sensors thus different strategies have been employed to achieve high stability for these assays. The interaction of biotin and streptavidin has been exploited in many protein and nucleic acid detection and purification methods. Biotin-binding proteins have been widely used for the immobilization of biotinylated DNA due to their high affinity ($K_d \sim 10^{-15}$), binding capacity, reproducibility, and chemical resistance [16, 30, 31, 32]. Furthermore, the biotin label is stable and small, it rarely interferes with the function of labeled molecules enabling this interaction to be used for the development of highly sensitive and stable assays.

A significant effort has been made to monitor and understand structural characteristics of DNA at surfaces such as size, shape, orientation. Xiaodi and colleagues studied the effect of a transcription factor that regulates gene expression by binding to a specific DNA sequence [33]. By using a combination of QCM-D and SPR methods, the group was able to distinguish different viscoelastic behavior between estrogen receptor/DNA complexes in the presence of ligands. Using the discrete molecule approach, conformation of surface-attached

DNA molecules has been measured. Acoustic measurements were able to discriminate DNA molecules of various shapes and sizes [10, 12]. This work verified the model which suggests that the acoustic ratio is related to the intinsic viscosity of biomolecules.

Proteins

Protein adsorption onto biomaterial surfaces plays an important role in understating fundamental aspects of biology (bacterial biofilm formation) [19, 18], as well as for clinical applications (implant surfaces). For example the amount of adsorbed protein onto a surface is crucial since it can cause promotion or resistance of cell attachment and further development [17, 34]. In the context of better understanding protein-protein and DNA-protein interactions several examples confirm the sensitivity of the QCM-D technology [35, 36]. Voight-based models have been used in many studies to determine characteristics of protein films on several surfaces such as thickness, density, shear elastic modulus and viscosity using [6, 35, 37].

Alternatively the discrete molecule approach has been used in order to obtain information about molecules as individuals . In the work of Milioni et al. [13], DNA anchors (21,50,76 or 85 bp long) were used to achieve suspended attachment of two different molecules. A spherical protein (streptavidin) and a DNA molecule (47 bp) were attached to the sensor surface. The model predicted correctly the shape and size of the molecules. This method has also proven to be successful for proteins that can be hardly analyzed by traditional structural tools. Intrinsically disordered proteins (IDPs) are known to lack a fixed three dimensional structure, making them difficult to study with methods such as X-ray crystallography. Acoustic measurements were able to follow expansion and contraction of such a protein in response to salt concentration[14]. Moreover the measurements verified the association between acoustic ratio $\Delta D/\Delta f$ and the different conformations of the protein. The two applications of the discrete particle model, point out the need of developing substrates in order to bind molecules with high specificity, in a suspended way.

1.2 Molecules under study: surface immobilization of DNA and Proteins

1.2.1 Capturing DNA

DNA is a chemically diverse macromolecule and thus offers many possible ways for its immobilization. For example the phosphates at the 5´-end as well as the hydroxyl group at the 3´-end are used to introduce several modifications for subsequent binding of the molecule. In principle there are three main strategies for DNA immobilization: physical adsorption, covalent bonding (or chemical adsorption) and the use of biotin-binding proteins (an analytical review for more details [38]). Physical adsorption results in different (sometimes unpredictable) arrangement of DNA molecules on the surface [39]. Covalent attachment can be achieved either by functionalization of DNA molecules or by modification of surfaces (glass, silica, gold, metals). For example DNA molecules can be modified with thiols or by using peptide or carbon linkers. Cholesterol has been also used as a DNA tag [40]. This

modification allowed lateral diffusion of DNA molecules on Supported Lipid Bilayers (SLBs) in a rapid and stable manner.

1.2.2 Capturing Proteins

Surface immobilization of proteins can affect greatly their structure, function and dynamics. Often protein molecules are physically adsorbed onto surfaces, mainly through hydrophobic interactions, to form protein films. However there has been discussion on whether these proteins continue to be active and maintain their native structure [41]. Covalent attachment through spacers and thiolation methods is also possible on gold surfaces[42], allowing a more controlled binding of the molecules. Another common way is the biotinylation of a protein and subsequent immobilization either directly onto surfaces or on layers that contain biotin-binding proteins [43]. An alternative way is the use of His-tags which are mainly used during the protein purification [44, 14]. NTA containing surfaces allow the immobilization of the recombinant protein. The former two methods allow for immobilization that does not affect directly the native structure of the protein.

Molecule of study: Early Endosomal Antigen 1 (EEA1)

Role in Endocytosis

Cells need to continually adjust their membrane composition in order to communicate and respond to changes of the environment. By the process of endocytosis, components are transferred from the plasma membrane to endosomes (membrane bound transport vesicles). From there, components can either be recycled on the plasma membrane or be transferred to lysosomes for degradation. Endosomes can be distinguished in classes (early, late, recycling) and participate in a range of processes (apart from sorting and trafficking) such as cytokinesis, pollarization, migration and cell signaling [45].

The role of different classes of endosomes inside the cell is highly depended on their composition. A unique feature that distinguishes these classes is the presence of Phosphatidyl inositol phosphate (PIP) lipids. In particular phosphatidylinositol 3-phosphate (PtdIns3P or PI3P) is mainly located in early endosomes while PI(3,5)P_2 in late endosomes. The transition between phosphorilation states of the lipids is made by the use of phosphoinositide kinases and phosphatases. Many proteins that contain specific motifs (i.e. FYVE and PX domains) can bind with hight afinity to these lipids [45, 46, 47].

Transport vesicles must be very accurate in order to recognize the correct target membrane for fusion. Rab proteins and Rab regulators play an important role during this selection process. Rab proteins are small, monomeric GTPases that belong to the the Ras superfamily. They swich between two conformations, an active form bound to GTP and an inactive bound to GDP. The conversion between GTP and GDP-bound form is catalyzed by an exchange factor, leading Rab to activation. Rab escort proteins bind only the GDP form while Rab effectors, only bind the GTP-bound form of Rab. Rab effectors vary greatly, some of them are motor proteins and other are tethering proteins that have long coiled-coil domains that can extend to link two membranes. Early endosomal antigen 1 (EEA1) is such an effector, it binds PI3P lipids and acts as a molecular link between membrane and Rab5[49]. EEA1

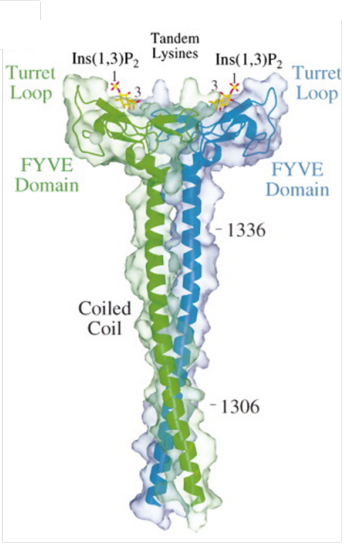

Figure 1.5: The polypeptide chains are colored green (chain A) and blue (chain B); the head group is shown in yellow (carbon and phosphorus atoms) and red (oxygen atoms) [48].

captures vesicles when being in its extended form while Rab 5 activates a change in flexibility of EEA1. As a result the EEA1 effector collapses, bringing the vesicles closer to the membrane [50].

Structural characteristics

EEA1 is localized in early endosomes and has a C-terminal region which binds to PI3Ps via a FYVE domain and a N-terminal region which interacts with Rab5 [48]. The C-terminal region is consisted of a coiled-coil, a stuctural motif of proteins, that end up to the FYVE domain and a C-terminal a helix that wraps around two Zn^{2+}. The recognition of PI3P lipid heads is made by conserved residues. The structure resembles the one of Vps27 and Hrs FYVE domains.

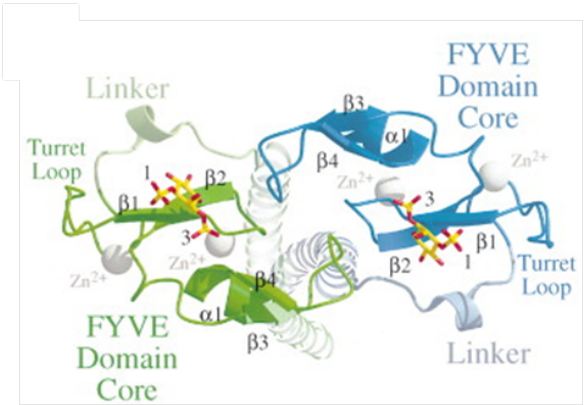

Figure 1.6: Top view with the linker regions in light green (chain A) and light blue (chain B) [48].

1.3 Aim of this study

Functionalization of surfaces is crucial for sensitive analysis of specific interactions between biomolecules. In this study two surfaces were designed for the immobilization of a) DNA molecules and b) EEA1, a protein that binds to PI3P lipids via its C terminal FYVE domain.

Objective 1: Design of a sophisticated surface for capturing DNA molecules.

A new surface was designed for the attachment of DNA molecules. Compared to neutravidin films that were previously used, this method allows the control of surface density and the suspension of grafted molecules.

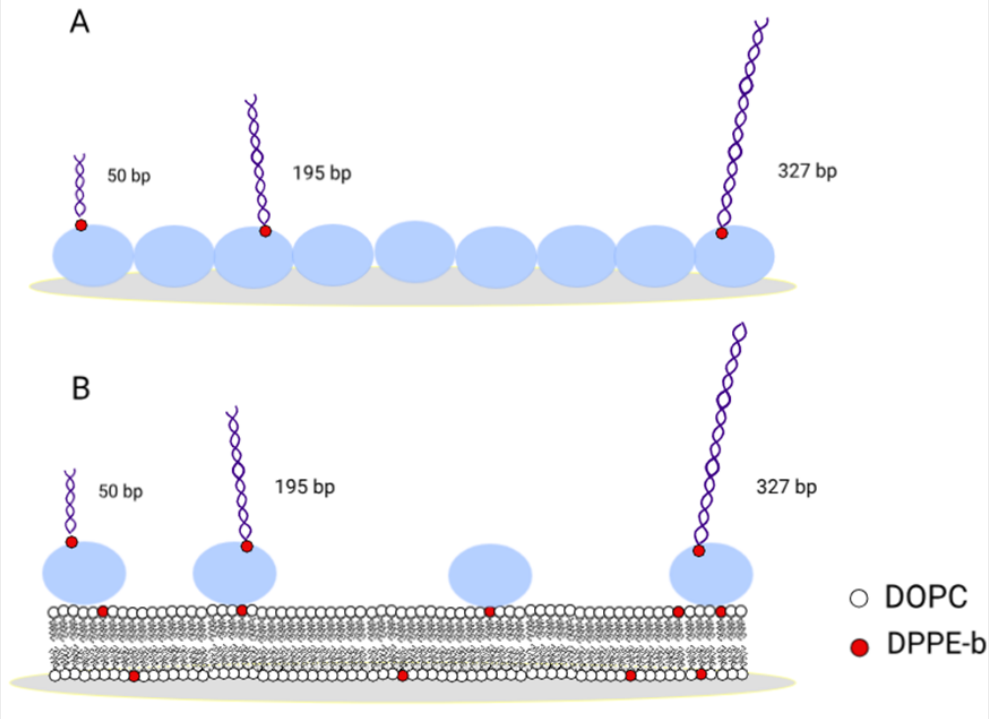

Figure 1.7: Schematic representation of the experimental architecture. Upper scheme (A) demonstrates various lengths of DNA molecules attached on a neutravidin film. (B) demonstrates a biotin containing lipid bilayer with attached streptavidin molecules, as an anchor for immobilizing DNA molecules of various lengths.

In order to elucidate the effect of the binding surface on the acoustic measurements of DNA molecules, we used SLBs containing biotinylated lipid heads (0.3-5%). The bilayers were formed allowing the binding of Streptavidin molecules. The biotin-binding protein was used for the immobilization of biotinylated DNA molecules of various lengths (50bp-635bp). The acoustic ratio of the target molecule was measured as a function of different mass coverage of the surface.

Objective 2: Establish the conditions for stable binding through PI3P and POPS lipids.

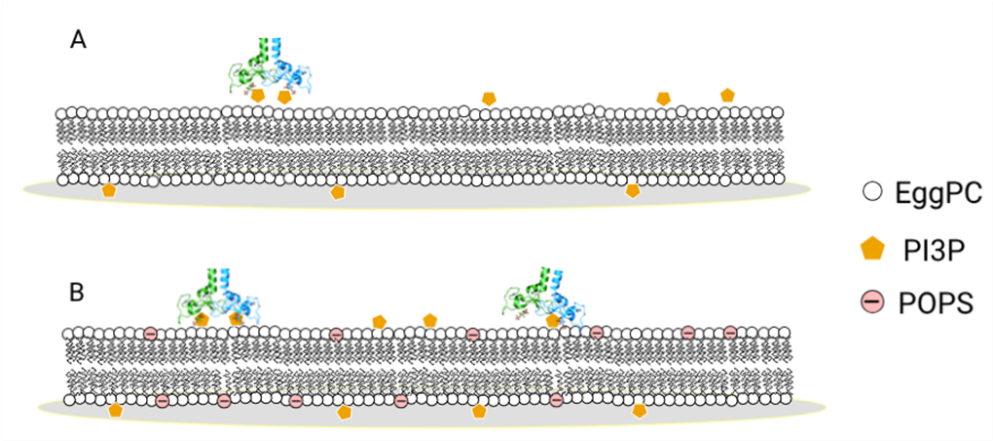

Figure 1.8: Schematic representation of the experimental architecture. (A): Bilayers containing EggPC and PI3P lipids for capturing EEA1 constructs. (B) Bilayers with EggPC, PI3P and POPS lipids for the attachment of EEA1 protein.

In the case of EEA1, a protein that specifically binds PI3P lipids, three protein constructs of similar molecular weight were analyzed. Various concentrations of constructs were immobilized on different lipid content SLBs and the binding capacity and stability was evaluated.

2 Materials and Methods

2.1 Liposome preparation

1,2-dioleoyl-sn-glycero-3-phosphocholine (DOPC), 1,2-dioleoyl-sn-glycero- 3-phosphoethanolamine-N-(cap biotinyl) (DPPE-b), L-a-phosphatidylcholine from egg chicken (EggPC), 1-palmitoyl-2-oleoyl-sn-glycero-3-phospho-L-serine (POPS) lipids were purchased from Avanti Polar Lipids (Alabaster, Al, USA). Dipalmitoyl Phosphatidylinositol 3-phosphate (PI3P) lipids were purchased from Echelon Biosciences Incorporated (EBI). Lyophilized lipids were dissolved in 1:1 chloroform:methanol to a final concentration of 10 mg/ml or in the case of PI3P in 1:2:0.6 chloroform:methanol:water to a final concentration of 0.666mg/ml. Stock solutions were placed in glass vials and stored at -20°C. For DNA studies, DOPC:DPPE-b lipids were mixed in the desired amount ranging from 5 to 0.3% of DPPE-b, while for protein studies the lipid ratios were EggPC:PI3P (95:5, 90:10, n/n) and EggPC:POPS:PI3P (80:15:5, n/n). The organic solvent was first evaporated under a gentle stream of nitrogen while gently turning the flask to form a thin lipid film onto the wall of the flask, and then further dried under nitrogen for 30 minutes minimum. DOPC:DPPE-b lipid films were hydrated in TNa150 buffer: 10mM Trizma hydrochloride solution, pH: 7.5, 1M (Merck), 150mM NaCl (Riedel-de Haën- Honeywell International Inc.) at final concentration of 2mg/ml. EggPC:PI3P and EggPC:POPS:PI3P lipid films were prepared with T20Na150 buffer (20mM Trizma, 150 NaCl, 0.5mM TCEP). After vortexing for 30 minutes, the resulting multilamellar vesicle solutions were extruded 25 times through a polycarbonate membrane with 50-nm nominal pore diameter (LiposoFast, Avestin) leading to a stock solution of unilamellar vesicles which were stored at 4 °C and used for 5 to 7 days at maximum.

2.2 Amplification of DNA fragments

Different lengths of double stranded DNA were prepared either by PCR amplification using Human DNA (Takara Bio Inc.) or *Salmonella enterica* DNA as template. In the case of the 50 bp DNA, direct hybridization to the complementary sequence was used. All DNA fragments (50bp, 88bp, 195bp, 327bp, 446bp and 635bp) had a biotin attached to the 5' prime end. The amplified fragments were further cleaned using a NucleoSpin PCR Clean-up kit (Macherey-Nagel) and their purity was checked by 2% agarose gel electrophoresis.

2.3 Protein purification-constructs

The soluble constructs of C terminal EEA1-GFP, C terminal EEA1-mcherry and 2xFYVE-GFP were provided by Marino Zerial's Group (Max Planck Institute of Molecular Cell biology & Genetics, Dresden, Germany) and stored at -20°C.

2.4 Quartz Crystal Microbalance with Dissipation monitoring (QCM-D)

A QCM-D (Q-Sense E4, Sweden) was used to measure changes in resonance frequency Δf and dissipation ΔD. Measurements presented here were performed at operating frequency of 35MHz (i.e., seventh overtone), with a continuous flow rate of 50 μl/min and temperature of 25°C. SiO_2 coated sensors (Q-Sense QSX 303) were cleaned with Hellmanex 2%, rinsed with miliQ water, dried under nitrogen stream, and were then either treated for 2.5 minutes using a plasma cleaner (Harrick PDC-002, USA) or for 20 minutes using a UV ozone cleaner (Ossila, UK) to ensure hydrophilic surfaces.

2.5 Real-time acoustic detection of DNA and protein binding

A continuous flow of TNa150 buffer was pumped through the QCM-D chambers and the acoustic signal was allowed to equilibrate prior to the first addition. a) DOPC:DPPE-b SLBs were formed upon injection of 0.05 mg/ml lipid solution using the same buffer. After lipid bilayer formation and stabilization of the acoustic signal, streptavidin was injected. The protein was diluted at a final concentration of 10 μg/ml and the binding to the bilayer was recorded. After buffer injection and stabilization of signal, biotinylated DNA fragments were injected at various concentrations. Both streptavidin and DNA were dissolved in the same buffer used for liposome and SLB formation. b) EggPC:PI3P and EggPC:POPS:PI3P SLBs were formed upon injection of 0.05 mg/ml or 0.1mg/ml lipid solution using the same buffer. After lipid bilayer formation and stabilization of the acoustic signal, EEA1 C-terminal constructs were injected at different concentrations (0.1 to 3.5μM for Ct-EEA1-GFP, 0.5 to 2.5 μM for Ct-EEA1-mCherry and 0.04 to 2 μM for 2xFYVE-GFP). Buffer exchanges followed each binding step. Finally the ratio of dissipation to frequency change (ΔD/Δf) was calculated and plotted as a function of bound molecule coverage.

3 Results

3.1 Results for Immobilization of DNA molecules

For the DNA attachement, first SLBs containing DPPE-b lipids were formed (Fig. 3.1, I), followed by the binding of streptavidin (Fig. 3.1, II). Finally DNA was injected (Fig. 3.1, III). Each step of the experiment is discussed in detail in the next section.

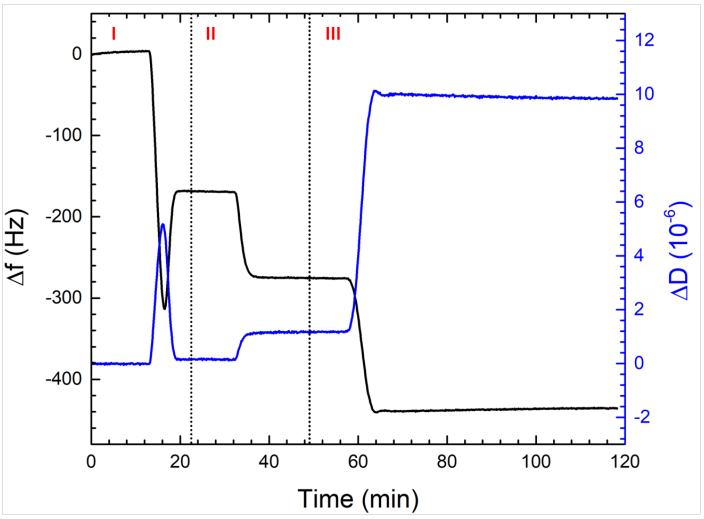

Figure 3.1: Representative experiment showing the steps for anchoring DNA. (I) SLB formation, (II) Streptavidin attachment and (III) DNA binding

3.1.1 Supported Lipids Bilayer (SLB) formation

In this work we used a SLB platform to tether biotinylated DNA molecules. It is important for the application of discrete particle model, that the attached biomolecules do not interact with the surface or its neighboring molecules. For that reason different fractions of DOPC and DPPE-b lipids were mixed in the desired amount, DOPC:DPPE-b (99.7:0.3, 99.5:0.5, 99.3:0.7, 99:1, 95:5, mol/mol) for the formation of liposomes. SLBs were formed upon addition of 0.05 mg/ml lipid solution with a final frequency and dissipation change Δf = -170 Hz and $\Delta D = 0.13 \times 10^{-6}$. These values are typical and confirm the formation of a homogeneous lipid bilayer [51]. Further injection of BSA (0.1 mg/ml) verified the presence of a complete bilayer (not shown).

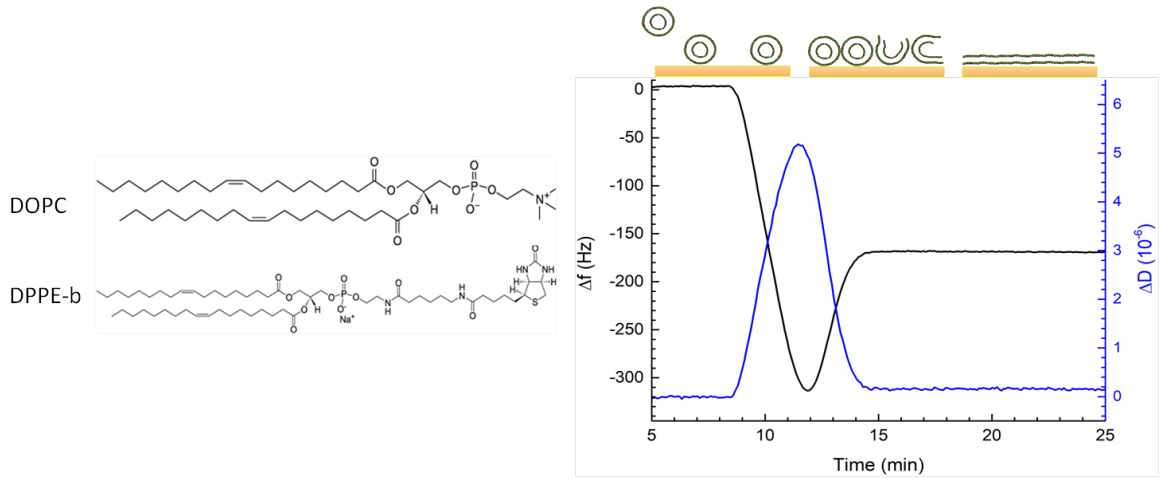

Figure 3.2: Chemical structure of DOPC and DPPE-b lipids and SLB formation. The liposomes reached a critical concentration (lowest and highest peak of frequency and dissipation respectively), before the formation of the planar bilayer.

Minimum frequency and maximum dissipation is observed, (indicating the critical concentration of SUVs on the surface) followed by rupture and formation of the bilayer.

3.1.2 Streptavidin attachment

After the formation of SLBs with DPPE-b content and rinsing with TNa150 buffer, SAv was injected (10 μg/ml) until saturation and equilibration of the signal. A range of SAv coverages were tested in order to achieve stability of binding. Δf were used as estimation of mass per unit area based on Sauerbrey. ΔD/Δf ratio was calculated to estimate the dependence with the surface coverage and to separate its contribution from the proceeding steps (binding of DNA molecules).

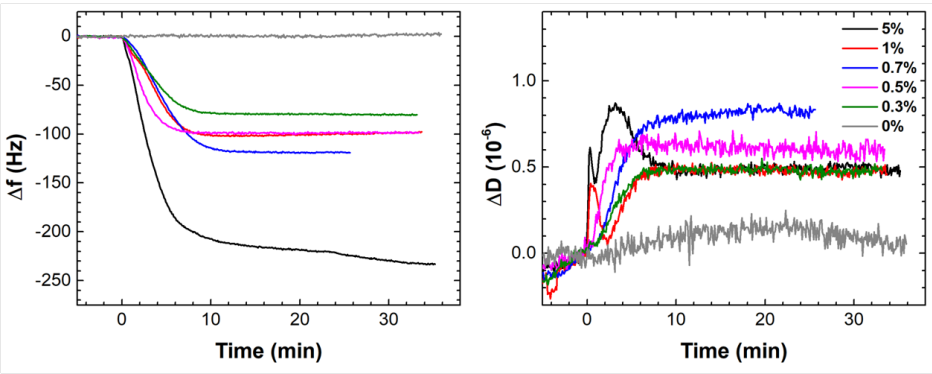

Figure 3.3: Streptavidin attachment on bilayers with different fraction of biotinylated lipid heads.

As shown in fig.3.4, variation of Streptavidin coverage did not affect the acoustic ratio (ΔD/Δf) of the protein and we can therefore assume that there is no correlation between them.

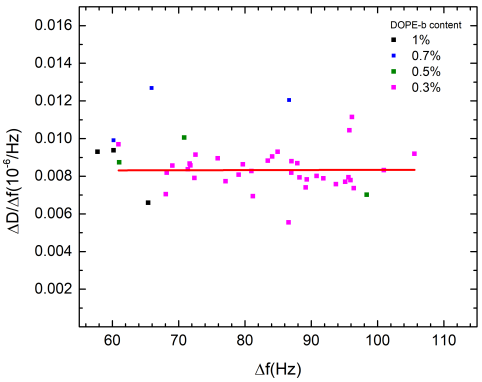

Figure 3.4: Dependence of the acoustic ratio on surface coverage of SAv. Each point corresponds to a single experiment measured at equilibrium.

3.1.3 DNA binding on streptavidin attached to the SLB

Different concentration of DNA was used in order to achieve a range of different surface coverages. To assure that the DNA molecules bound specifically on streptavidin (and not to plain SLBs), biotinylated DNA was also pumped over a SLB surface with no streptavidin molecules (fig. 3.5, (A), black line); DNA specifically bound only when streptavidin was present and not on bilayers. The ratio $\Delta D/\Delta f$ was calculated and plotted versus the corresponding frequency as shown in fig. 3.5, (B). The acoustic ratio is coverage dependent and a linear fit was performed for each DNA length. The fit parameters are written in fig. 3.5, (B).

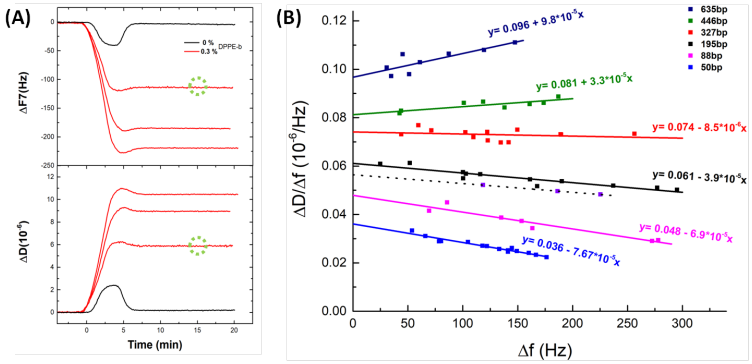

Figure 3.5: a: Binding of biotinylated DNA (195bp) on surfaces containing 0 and 0.3% of DPPE-b. Surfaces with 0% DPPE-b were used as a control and did not bind SAv or biotinylated DNA. $\Delta D/\Delta f$ ratio was calculated for each experiment and plotted versus Δf (time point in green circles). b: Acoustic ratio, $\Delta D/\Delta f$ dependence on DNA coverage. Each color corresponds to different DNA length. Surfaces with 5% DPPE-b were also evaluated for DNA 195bp (black-dashed line).

3.2 Results for capturing of EEA1 C-terminal constructs

For the attachment of EEA1 constructs we used SLBs with different lipid compositions. After the formation of the bilayers (fig. 3.6, I), protein was injected (fig. 3.6, II) and the binding stability was followed. In next section, each step is described separately in detail.

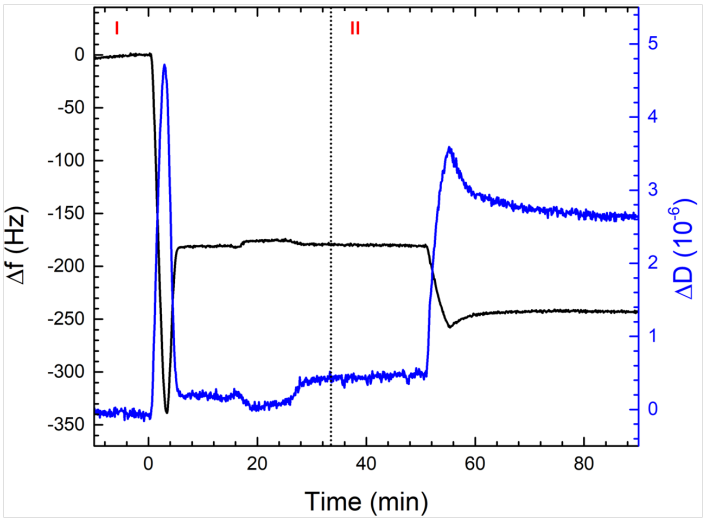

Figure 3.6: Real-time representative sensogram when capturing EEA1 constructs. (I) SLB formation and (II) Ct-EEA1 binding

3.2.1 SLB formation

For the immobilization of Ct-EEA1 constructs different liposome compositions were tested for the bilayers, containing PI3P and/or PS lipids. The final frequency and dissipation changes were recorded upon addition of 0.05mg/ml lipid solution and buffer rinsing (Δf = -170Hz, ΔD= 0.3*10^{-6}).

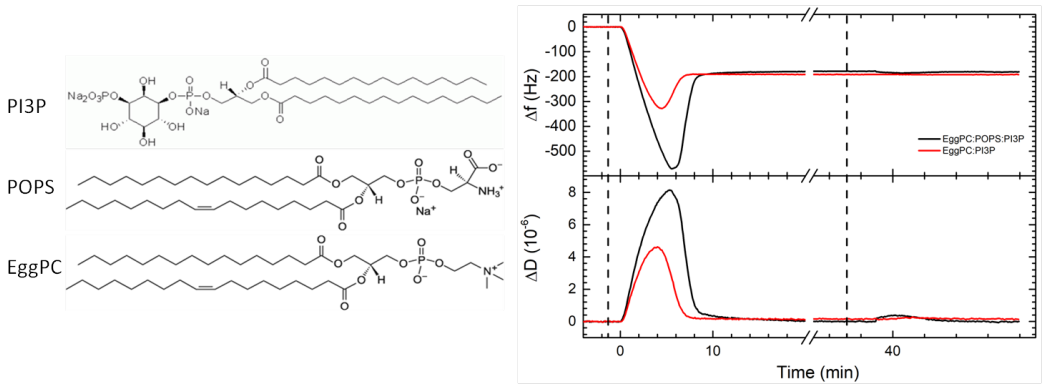

Figure 3.7: Chemical structure of lipids used for the formation of SLBs and a characteristic QCM-D signature of SLB formation using SUVs. Minimum frequency and maximum dissipation is observed before the formation of the bilayer. Black and red lines show formation of bilayer with and without POPS lipid respectively.

Both EggPC:PI3P and EggPC:POPS:PI3P bilayers were treated with 0.1mg/ml Bovine Serum Albumin (BSA), which was used as a control. No significant signal was recorded (Δf $\sim$ 1Hz), confirming the formation of a continuous bilayer. Comparison of bilayers rupture ability with and without POPS, a negatively charged lipid, show a great difference in the kinetics of bilayer formation (fig. 3.7). In the presence of POPS, liposome rupture occurs after a much higher frequency pick (indicates the onset of the bilayer formation) of ~ -600 Hz, compared to EggPC:PI3P liposomes where Δf minimum is ~ -300 Hz. Increase of lipid concentration (0.1 mg/ml) was also tested but did not affect significantly the kinetics or the final values.

3.2.2 Binding of EEA1 constructs to different SLB compositions

Binding of constructs to SLBs with no PI3P lipids

As a first step, to ensure the specificity of the protein binding to PI3P lipids, plain EggPC bilayers were tested. In the case of Ct-EEA1-GFP and 2xFYVE-GFP no binding was recorded confirming the specific interaction of PI3P lipids with the FYVE domains. For Ct-EEA1-mCherry the results suggest that non specific binding occurs ($\Delta f_{0\%PI3P}$ is almost the same as $\Delta f_{5\%PI3P}$).

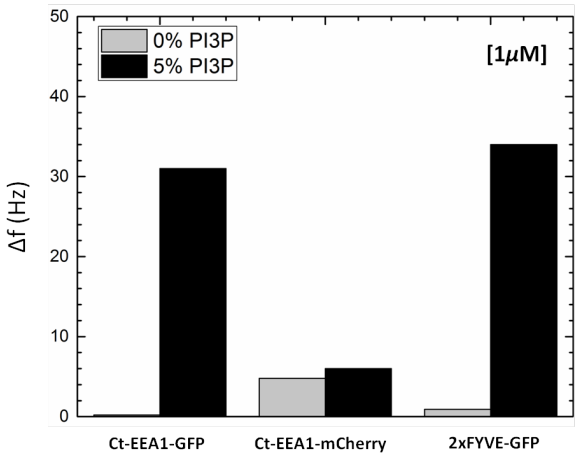

Figure 3.8: Binding of EEA1 constructs to SLBs with and without PI3P content. Δf is obtained upon injection of 1μM (400μl). For Ct-EEA1-GFP and 2xFYVE-GFP, Δf is less that 1Hz. Ct-EEA1-mCherry binds non specifically to the bilayers.

The C-terminal of EEA1 is characterized by two functional domains: one that binds to the active, GTP-bound form of the early-endosomal GTPase Rab5 and a FYVE finger that binds to PI3P lipids. The FYVE domain and its specific interaction with PI3P lipids were used for the immobilization of three EEA1 constructs. Lipid surfaces were evaluated using the three constructs and their binding capacity, specificity and stability were tested. SLBs were formed containing different ratios of EggPC, PI3P and POPS lipids. The three constructs were: C terminal of EEA1 fused with GFP (Ct-EEA1-GFP), C terminal of EEA1 fused with mCherry (Ct-EEA1-mCherry) and 2xFYVE domain fused with GFP (2xFYVE-GFP). The three constructs of similar size, $\sim$ 73 KDa were first checked for aggregations by native gel.

Binding of EEA1 constructs on SLBs with 5% PI3P lipids

For the immobilization of C-terminal construct SLBs containing Egg-PC:PI3P (95:5, mol/-mol) were first used as shown in Figure 3.7. For Ct-EEA1-GFP, a range of protein concentration was used (0.5-3.37 μM) to determine the minimum and maximum amount of protein that can be bound to the surface. The stability of protein binding was followed at least for 30 minutes after the addition of 400 μl protein solution. Each step was followed by buffer rinsing to evaluate the binding stability. A small desorbtion was recorded probably due to non stable binding of the protein on the surface. For each protein concentration, Δf values were plotted in a titration curve (fig. 3.9, right panel).

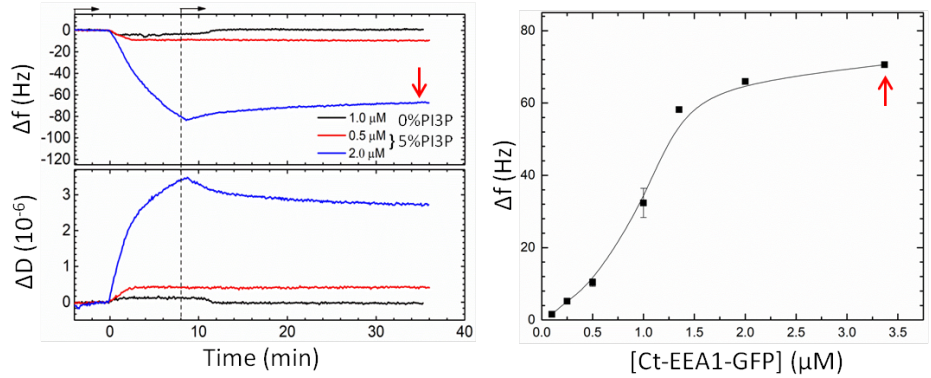

Figure 3.9: Left panels show frequency and energy dissipation obtained upon addition of 0.5μM and 2 μM (400 μl), followed by buffer rinsing (dashed vertical line). Red arrow on the left panel indicates Δf used in titration curves (all obtained after 40 minutes of equilibration).

The binding of C terminal-mCherry on EggPC:PI3P (95:5, mol/mol) was also examined. As shown in figure 3.10, even at high concentrations of 2.5 μM (Δf $<$ 30Hz) the binding was very low ($\sim$ 20 Hz). In addition, binding of the protein (1 μM) on bilayers containing only EggPC lipids, showed non specific interactions (fig. 3.10) indicating that binding is not mediated by PI3P lipids.

2xFYVE-GFP is an artificial construct, lucking the coiled-coil domain of EEA1. It is composed of two tandem FYVE-finger domains, joined trough a linker. 2xFYVE-GFP binds PI3P with high specificity [46]. A range of concentrations 44nM to 2 μM was injected on EggPC:PI3P (95:5, mol/mol) bilayers. After buffer rinsing a big step of adsorption is observed $\sim$ 40 Hz indicating a non stable interaction between the construct and PI3P lipids. Therefore the results indicate high binding capacity but low stability.

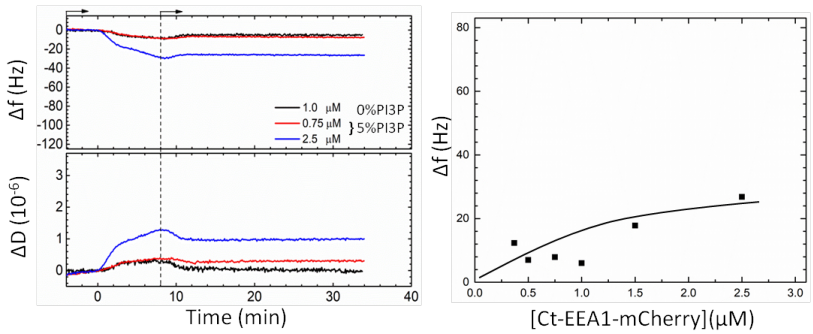

Figure 3.10: Changes in frequency (top-left panel) and energy dissipation (bottom-left panel) obtained upon addition of 0.75μM and 2.5 μM (minimum and maximum detection of Ct-EEA1-mCherry construct), followed by buffer rinsing (dashed vertical line). Black line shows the binding specificity of the construct on bilayer containing EggPC lipids. Right panel: titration curve obtained for stable protein binding after buffer rinsing (black line drawn to guide the eye).

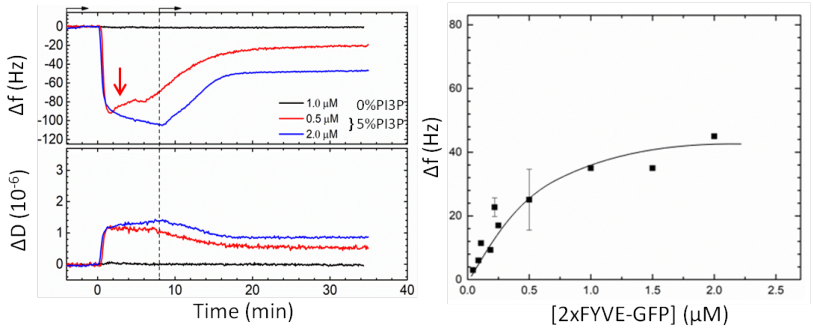

Figure 3.11: Left: changes in frequency and dissipation obtained upon addition of 0.5μM and 2 μM construct concentration, followed by buffer rinsing (dashed line). Red arrow indicates the unbinding of molecules from the surface. Right: Titration curve for 2xFYVE-GFP (black line is drawn to guide the eye).

Binding of EEA1 constructs on SLBs with increased PI3P content

In an attempt to enhance the protein binding and stability after rinsing, the amount of PI3P lipids was increased and the bilayers were again tested. Liposomes containing 10% of PI3P lipids were produced and after the SLB formation, the binding was recorded. In this set of experiments only low protein concentration was tested (i.e. 0.25 and 0.5 μM, Figure 3.11). In the case of Ct-EEA1-mCherry 1μM was also tested. Ct-EEA1-GFP binding was enhanced only for the higher concentration. An almost three-fold difference was obtained between bilayers containing 5 % and 10 % PI3P lipids ($\Delta f_{5\%}$= 10Hz, $\Delta f_{10\%}$= 30Hz). In the case of 0.25 μM, no significant difference was recorded for frequency or dissipation. The binding of Ct-EEA1-mCherry was not affected for concentrations of 0.25 and 0.5 μM, but only at 1μM (fig.3.12, (B)). 2xFYVE-GFP showed different binding kinetics when binding to EggPC:PI3P (90:10, mol/mol). At first a distinguishable difference is observed, both for 0.25 and 0.5 μM (fig 3.11, b), however after buffer rinsing (dashed line) the amount of bound

molecules washes off, leaving almost the same bound molecules as on EggPC:PI3P (95:5, mol/mol).

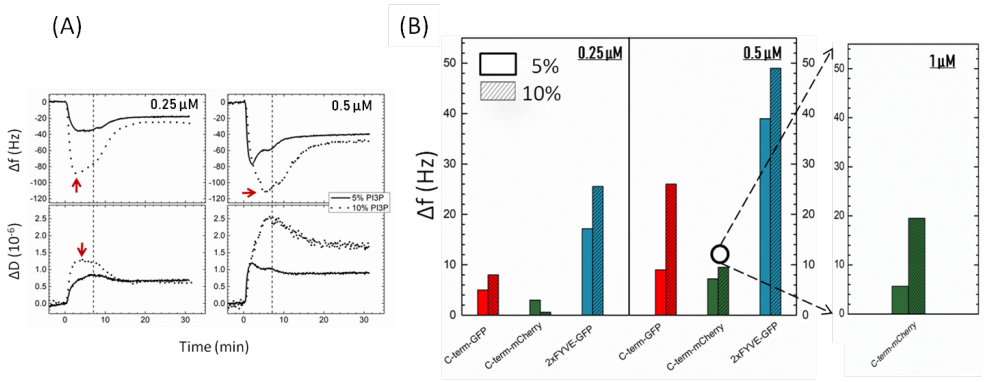

Figure 3.12: (a) Δf obtained for three constructs (red: Ct-EEA1-GFP, green: Ct-EEA1-mCherry, blue: 2xFYVE-GFP) binding to SLBs with 5 and 10% PI3P lipids (striped lines). Two concentrations were tested for Ct-EEA1-GFP and 2xFYVE-GFP (0.25 and 0.5 μM). (b) Real-time binding of 2xFYVE-GFP construct on SLBs containing 5 and 10% PI3P lipids. Although change in signal is observed in an initial stage (red arrow), final values (after rinsing with buffer, dashed line) do not differ significantly.

Binding of Ct-EEA1-GFP on SLBs containing POPS lipids

In order to further optimize the protocol the effect of POPS lipids on the binding of Ct-EEA1-GFP were tested. Liposomes containing negatively charged lipids were prepared with a lipid ratio as follows: EggPC:POPS:PI3P (80:15:5, mol/mol). Ct-EEA1-GFP binding was affected greatly by the presence of POPS lipid. For the concentration of 1 μM, the frequency was 98 and 30 Hz for bilayers with and without POPS respectively.

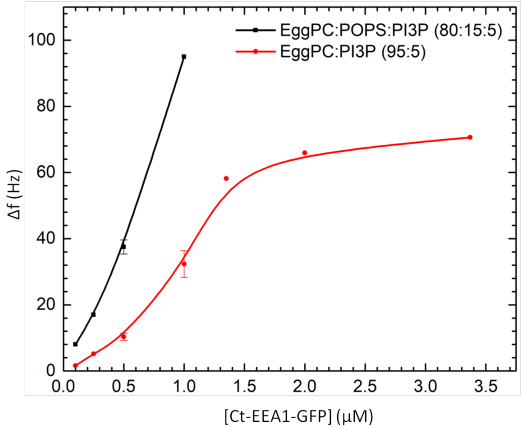

Figure 3.13: Comparison of titration curves for Ct-EEA1-GFP construct on EggPC:PI3P (95:5, mol/mol) and EggPC:POPS:PI3P (85:15:5, mol/mol).

4 Discussion

4.1 DNA binding through a biotin-streptavidin interaction on SLBs

We have investigated the effect of a linker, particularly a SLB with Streptavidin attached, between our surface and a target biotinylated DNA. In previous work the acoustic ratio of nucleic acids which were all single-point attached to neutravidin layer directly adsorbed on gold was measured [12]. $\Delta D/\Delta f$ ratios that were obtained experimentally, verified the theoretical relationship between acoustic ratios and $[\eta]$ [10]. Most importantly $\Delta D/\Delta f$ ratio showed no dependence with the DNA coverage. In our case the surface binding strategy affects the acoustic ratio. While the acoustic ratio of streptavidin bound to a SLB was not affected by the coverage (fig. 3.4), the acoustic ratio of DNA molecules behaved differently (fig. 3.5 (B)).

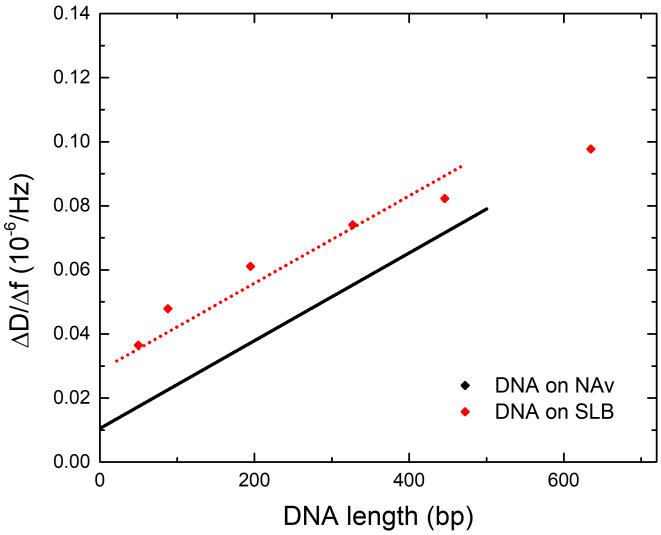

Figure 4.1: Acoustic ratio, $\Delta D/\Delta f$ as a function of DNA length. A straight line extrapolation to zero DNA length (fig. 3.5 (B)) leads to a Y-axis intercept corresponding to the ratio of each DNA length. Black dots represent the ratios of DNA molecules that are bound to neutravidin-modified surface. The values are obtained using the equation (7) from [12]. Red dots represent the acoustic ratio for DNA molecules on a SLB containing streptavidin molecules.

From this study it appears that linker has a great impact on $\Delta D/\Delta f$ ratio when comparing to previous work. When bound to an SLB, DNA acoustic ratio depends highly on

surface coverage. On the other hand there seems to be no correlation between the acoustic ratio of the Streptavidin with the protein's coverage; data may also suggest that supported membranes could provide higher sensitivity for the immobilization of appropriately modified DNA molecules. Further analysis and research should be done in order to understand the physics behind the acoustic behavior of the each time employed linker.

4.2 EEA1 C-terminal constructs capture on SLBs

SLB formation was an important step for enhancement and stability of construct immobilization. We were able to identify the amount of protein that irreversibly binds to PI3P-containing SLBs as well as the specificity in the absence of the mediating lipid. The three constructs behaved in a different way, even though they have similar size ($\sim$ 73 KDa) and all contain the FYVE domain that is required for specific attachment. The constructs differed considering their binding affinity, specificity and kinetics. Firstly, SLBs containing Egg PC 95% and PI3P 5% and SLBs of 100% EggPC were prepared and used for protein binding. Ct-EEA1-mCherry bound insufficiently (fig. 3.10) and non-specifically, since binding was observed in the absence of PI3P lipids (fig. 3.8). Ct-EEA1-GFP and 2xFYVE-GFP demonstrated a different behavior, both of them bound specifically to PI3P lipids although the binding was affected after buffer rinsing and the maximum amount of protein that remained bound to the bilayer was relatively low ($\sim$ 70Hz). Increase of PI3P lipid fraction (10%) enhanced the binding of Ct-EEA1-GFP while 2xFYVE-GFP, after buffer rinsing, the binding was almost the same as the binding to SLBs with 5% PI3P lipid. While PI3P lipids are known to be the link between endosome membranes and FYVE domains, these results indicate that addition of POPS (negatively charged) lipids enhance the binding of Ct-EEA1-GFP construct (fig. 3.13).

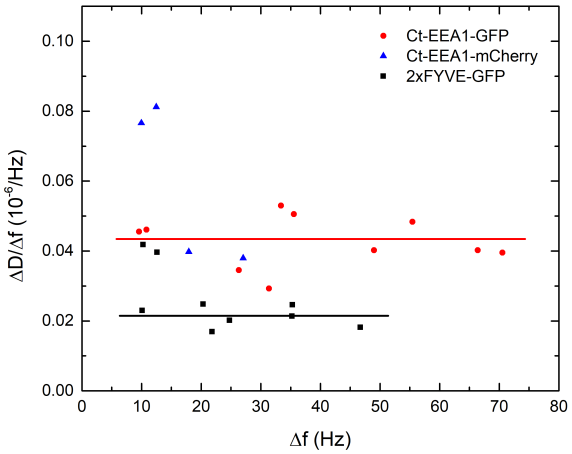

Figure 4.2: Acoustic ratios of EEA1 constructs. Ct-EEA1-GFP and 2xFYVE-GFP have different shapes and thus distinct acoustic ratios.

The acoustic ratios of the three constructs were calculated and plotted as a function of Δf

(fig. 4.2). These preliminary data show no correlation between surface coverage and acoustic ratio, at least for $\Delta f \sim 70$ Hz, for Ct-EEA1-GFP and 2xFYVE-GFP. Furthermore there is a distinction of the acoustic ratio of the two constructs, Ct-EEA1-GFP and 2xFYVE-GFP. As mentioned before, in Ct-EEA1-GFP, the FYVE domains are joined through the coiled-coil domain of EEA1. This characteristic does not apply for 2xFYVE-GFP, since the construct is artificially bound with a linker and lacks the coiled-coil part. The two constructs have different shapes and it is therefore expected that the acoustic ratio of 2xFYVE-GFP is less than that of Ct-EEA1-GFP.

List of Acronyms

QCM-D	Quarz Crystal Microbalance with Dissipation Monitoring
SPR	Surface Plasmon Resonance
SLB	Supported Lipid Bilayer
EEA1	Early Endosomal Antigen 1
SUV	Small Unilamellar Vescicles
SALB	Solvent Assisted Lipid Bilayer
PIPs	phosphatidylinositol phosphates
GTP	Guanosine triphosphate
GDP	Guanosine diphosphate
SAv	Streptavidin

Bibliography

[1] Nam-Joon Cho, Kay K. Kanazawa, Jeffrey S. Glenn, and Curtis W. Frank. Employing two different quartz crystal microbalance models to study changes in viscoelastic behavior upon transformation of lipid vesicles to a bilayer on a gold surface. *Analytical Chemistry*, 79(18):7027–7035, sep 2007.

[2] Michael Rodahl, Fredrik Höök, Anatol Krozer, Peter Brzezinski, and Bengt Kasemo. Quartz crystal microbalance setup for frequency and q-factor measurements in gaseous and liquid environments. *Review of Scientific Instruments*, 66(7):3924–3930, jul 1995.

[3] Ilya Reviakine, Diethelm Johannsmann, and Ralf P. Richter. Hearing what you cannot see and visualizing what you hear: Interpreting quartz crystal microbalance data from solvated interfaces. *Analytical Chemistry*, 83(23):8838–8848, dec 2011.

[4] Coy McNew. The attachment of colloidal particles to environmentally relevant surfaces: Effect of ionic strength, particle shape, and physicochemical properties, 12 2015.

[5] M V Voinova, M Rodahl, M Jonson, and B Kasemo. Viscoelastic acoustic response of layered polymer films at fluid-solid interfaces: Continuum mechanics approach. *Physica Scripta*, 59(5):391–396, may 1999.

[6] Fredrik Höök, Bengt Kasemo, Tommy Nylander, Camilla Fant, Kristin Sott, and Hans Elwing. Variations in coupled water, viscoelastic properties, and film thickness of a mefp-1 protein film during adsorption and cross-linking: a quartz crystal microbalance with dissipation monitoring, ellipsometry, and surface plasmon resonance study. *Analytical Chemistry*, 73(24):5796–5804, dec 2001.

[7] Diethelm Johannsmann, Ilya Reviakine, and Ralf P. Richter. Dissipation in films of adsorbed nanospheres studied by quartz crystal microbalance (QCM). *Analytical Chemistry*, 81(19):8167–8176, oct 2009.

[8] Diethelm Johannsmann, Ilya Reviakine, Elena Rojas, and Marta Gallego. Effect of sample heterogeneity on the interpretation of QCM(-d) data: Comparison of combined quartz crystal microbalance/atomic force microscopy measurements with finite element method modeling. *Analytical Chemistry*, 80(23):8891–8899, dec 2008.

[9] Edurne Tellechea, Diethelm Johannsmann, Nicole F. Steinmetz, Ralf P. Richter, and Ilya Reviakine. Model-independent analysis of QCM data on colloidal particle adsorption. *Langmuir*, 25(9):5177–5184, may 2009.

[10] Achilleas Tsortos, George Papadakis, Konstantinos Mitsakakis, Kathryn A. Melzak, and Electra Gizeli. Quantitative determination of size and shape of surface-bound DNA using an acoustic wave sensor. *Biophysical Journal*, 94(7):2706–2715, apr 2008.

[11] Achilleas Tsortos, George Papadakis, and Electra Gizeli. Shear acoustic wave biosensor for detecting DNA intrinsic viscosity and conformation: A study with QCM-d. *Biosensors and Bioelectronics*, 24(4):836–841, dec 2008.

[12] Achilleas Tsortos, George Papadakis, and Electra Gizeli. On the hydrodynamic nature of DNA acoustic sensing. *Analytical Chemistry*, 88(12):6472–6478, jun 2016.

[13] Dimitra Milioni, Achilleas Tsortos, Marisela Velez, and Electra Gizeli. Extracting the shape and size of biomolecules attached to a surface as suspended discrete nanoparticles. *Analytical Chemistry*, 89(7):4198–4203, mar 2017.

[14] Pablo Mateos-Gil, Achilleas Tsortos, Marisela Vélez, and Electra Gizeli. Monitoring structural changes in intrinsically disordered proteins using QCM-d: application to the bacterial cell division protein ZipA. *Chemical Communications*, 52(39):6541–6544, 2016.

[15] Yoon-Kyoung Cho, Sunhee Kim, Young A Kim, Hee Kyun Lim, Kyusang Lee, DaeSung Yoon, Geunbae Lim, Y.Eugene Pak, Tai Hwan Ha, and Kwan Kim. Characterization of DNA immobilization and subsequent hybridization using in situ quartz crystal microbalance, fluorescence spectroscopy, and surface plasmon resonance. *Journal of Colloid and Interface Science*, 278(1):44–52, oct 2004.

[16] George Papadakis, Achilleas Tsortos, Florian Bender, Elena E. Ferapontova, and Electra Gizeli. Direct detection of DNA conformation in hybridization processes. *Analytical Chemistry*, 84(4):1854–1861, feb 2012.

[17] C. Wittmer, J. Phelps, W. Saltzman, and P. Vantassel. Fibronectin terminated multilayer films: Protein adsorption and cell attachment studies. *Biomaterials*, 28(5):851–860, feb 2007.

[18] J. Kreth, E. Hagerman, K. Tam, J. Merritt, D. T. W. Wong, B. M. Wu, N. V. Myung, W. Shi, and F. Qi. Quantitative analyses of streptococcus mutans biofilms with quartz crystal microbalance, microjet impingement and confocal microscopy. *Biofilms*, 1(4):277–284, oct 2004.

[19] Adam L.J. Olsson, Michael R. Mitzel, and Nathalie Tufenkji. QCM-d for non-destructive real-time assessment of pseudomonas aeruginosa biofilm attachment to the substratum during biofilm growth. *Colloids and Surfaces B: Biointerfaces*, 136:928–934, dec 2015.

[20] Monica Bianco, Alessandra Aloisi, Valentina Arima, Michela Capello, Sammy Ferri-Borgogno, Francesco Novelli, Stefano Leporatti, and Rosaria Rinaldi. Quartz crystal microbalance with dissipation (QCM-d) as tool to exploit antigen–antibody interactions in pancreatic ductal adenocarcinomadetection. *Biosensors and Bioelectronics*, 42:646–652, apr 2013.

[21] Özlem Ertekin, Selma Öztürk, and Zafer Öztürk. Label free QCM immunobiosensor for AFB1 detection using monoclonal IgA antibody as recognition element. *Sensors*, 16(8):1274, aug 2016.

[22] Gregory J. Hardy, Rahul Nayak, and Stefan Zauscher. Model cell membranes: Techniques to form complex biomimetic supported lipid bilayers via vesicle fusion. *Current Opinion in Colloid & Interface Science*, 18(5):448–458, oct 2013.

[23] C.A. Keller and B. Kasemo. Surface specific kinetics of lipid vesicle adsorption measured with a quartz crystal microbalance. *Biophysical Journal*, 75(3):1397–1402, sep 1998.

[24] Ralf Richter, Anneke Mukhopadhyay, and Alain Brisson. Pathways of lipid vesicle deposition on solid surfaces: A combined QCM-d and AFM study. *Biophysical Journal*, 85(5):3035–3047, nov 2003.

[25] Johan Karlsson, Saba Atefyekta, and Martin Andersson. Controlling drug delivery kinetics from mesoporous titania thin films by pore size and surface energy. *International Journal of Nanomedicine*, page 4425, jul 2015.

[26] Thanh H. Nguyen and Menachem Elimelech. Adsorption of plasmid DNA to a natural organic matter-coated silica surface: kinetics, conformation, and reversibility. *Langmuir*, 23(6):3273–3279, mar 2007.

[27] Thanh H. Nguyen and Menachem Elimelech. Plasmid DNA adsorption on silica: kinetics and conformational changes in monovalent and divalent salts. *Biomacromolecules*, 8(1):24–32, jan 2007.

[28] Tibor Hianik, Veronika Ostatná, Zuzana Zajacová, Ekaterina Stoikova, and Gennady Evtugyn. Detection of aptamer–protein interactions using QCM and electrochemical indicator methods. *Bioorganic & Medicinal Chemistry Letters*, 15(2):291–295, jan 2005.

[29] Jeffrey N. Murphy, Alan K. H. Cheng, Hua-Zhong Yu, and Dan Bizzotto. On the nature of DNA self-assembled monolayers on au: Measuring surface heterogeneity with electrochemical in situ fluorescence microscopy. *Journal of the American Chemical Society*, 131(11):4042–4050, mar 2009.

[30] Xiaodi Su, Ying-Ju Wu, and Wolfgang Knoll. Comparison of surface plasmon resonance spectroscopy and quartz crystal microbalance techniques for studying DNA assembly and hybridization. *Biosensors and Bioelectronics*, 21(5):719–726, nov 2005.

[31] Xiaodi Su, Ying-Ju Wu, Rudolf Robelek, and Wolfgang Knoll. Surface plasmon resonance spectroscopy and quartz crystal microbalance study of streptavidin film structure effects on biotinylated DNA assembly and target DNA hybridization. *Langmuir*, 21(1):348–353, jan 2005.

[32] Khin Moh Moh Aung, Xinning Ho, and Xiaodi Su. DNA assembly on streptavidin modified surface: A study using quartz crystal microbalance with dissipation or resistance measurements. *Sensors and Actuators B: Chemical*, 131(2):371–378, may 2008.

[33] Wendy Y.X. Peh, Erik Reimhult, Huey Fang Teh, Jane S. Thomsen, and Xiaodi Su. Understanding ligand binding effects on the conformation of estrogen receptor -DNA complexes: A combinational quartz crystal microbalance with dissipation and surface plasmon resonance study. *Biophysical Journal*, 92(12):4415–4423, jun 2007.

[34] Jenny Malmström, Hossein Agheli, Peter Kingshott, and Duncan S. Sutherland. Viscoelastic modeling of highly hydrated laminin layers at homogeneous and nanostructured surfaces: quantification of protein layer properties using QCM-d and SPR. *Langmuir*, 23(19):9760–9768, sep 2007.

[35] Jia Xu, Kai-Wei Liu, Kathleen S. Matthews, and Sibani L. Biswal. Monitoring DNA binding to escherichia coli lactose repressor using quartz crystal microbalance with dissipation. *Langmuir*, 27(8):4900–4905, apr 2011.

[36] Xiaoyong Wang, Chada Ruengruglikit, Yu-Wen Wang, and Qingrong Huang. Interfacial interactions of pectin with bovine serum albumin studied by quartz crystal microbalance with dissipation monitoring: Effect of ionic strength. *Journal of Agricultural and Food Chemistry*, 55(25):10425–10431, dec 2007.

[37] Hiroyuki Furusawa, Mayu Komatsu, and Yoshio Okahata. In situ monitoring of conformational changes of and peptide bindings to calmodulin on a 27 MHz quartz-crystal microbalance. *Analytical Chemistry*, 81(5):1841–1847, mar 2009.

[38] Robert A. Meyers, editor. *Encyclopedia of Analytical Chemistry*. John Wiley & Sons, Ltd, sep 2006.

[39] Peter E. Vandeventer, Jorge Mejia, Ali Nadim, Malkiat S. Johal, and Angelika Niemz. DNA adsorption to and elution from silica surfaces: Influence of amino acid buffers. *The Journal of Physical Chemistry B*, 117(37):10742–10749, sep 2013.

[40] Alexander Johnson-Buck, Shuoxing Jiang, Hao Yan, and Nils G. Walter. DNA–cholesterol barges as programmable membrane-exploring agents. *ACS Nano*, 8(6):5641–5649, may 2014.

[41] Willem Norde. My voyage of discovery to proteins in flatland ... and beyond. *Colloids and Surfaces B: Biointerfaces*, 61(1):1–9, jan 2008.

[42] Yung-Chuan Liu, Chih-Ming Wang, and Kuang-Pin Hsiung. Comparison of different protein immobilization methods on quartz crystal microbalance surface in flow injection immunoassay. *Analytical Biochemistry*, 299(2):130–135, dec 2001.

[43] Erik Nilebäck, Laurent Feuz, Hans Uddenberg, Ramūnas Valiokas, and Sofia Svedhem. Characterization and application of a surface modification designed for QCM-d studies of biotinylated biomolecules. *Biosensors and Bioelectronics*, 28(1):407–413, oct 2011.

[44] Ruth E. Baltus, Kendra S. Carmon, and Linda A. Luck. Quartz crystal microbalance (QCM) with immobilized protein receptors: comparison of response to ligand binding for direct protein immobilization and protein attachment via disulfide linker. *Langmuir*, 23(7):3880–3885, mar 2007.

[45] Gwyn W. Gould and Jennifer Lippincott-Schwartz. New roles for endosomes: from vesicular carriers to multi-purpose platforms. *Nature Reviews Molecular Cell Biology*, 10(4):287–292, mar 2009.

[46] D. J. Gillooly. Localization of phosphatidylinositol 3-phosphate in yeast and mammalian cells. *The EMBO Journal*, 19(17):4577–4588, sep 2000.

[47] Jean-Michel Gaullier, Anne Simonsen, Antonello DArrigo, Bjørn Bremnes, Harald Stenmark, and Rein Aasland. FYVE fingers bind PtdIns(3)p. *Nature*, 394(6692):432–433, jul 1998.

[48] John J. Dumas, Eric Merithew, E. Sudharshan, Deepa Rajamani, Susan Hayes, Deirdre Lawe, Silvia Corvera, and David G. Lambright. Multivalent endosome targeting by homodimeric EEA1. *Molecular Cell*, 8(5):947–958, nov 2001.

[49] Anne Simonsen, Roger Lippe, Savvas Christoforidis, Jean-Michel Gaullier, Andreas Brech, Judy Callaghan, Ban-Hock Toh, Carol Murphy, Marino Zerial, and Harald Stenmark. EEA1 links PI(3)k function to rab5 regulation of endosome fusion. *Nature*, 394(6692):494–498, jul 1998.

[50] David H. Murray, Marcus Jahnel, Janelle Lauer, Mario J. Avellaneda, Nicolas Brouilly, Alice Cezanne, Hernán Morales-Navarrete, Enrico D. Perini, Charles Ferguson, Andrei N. Lupas, Yannis Kalaidzidis, Robert G. Parton, Stephan W. Grill, and Marino Zerial. An endosomal tether undergoes an entropic collapse to bring vesicles together. *Nature*, 537(7618):107–111, aug 2016.

[51] Nam-Joon Cho, Curtis W Frank, Bengt Kasemo, and Fredrik Höök. Quartz crystal microbalance with dissipation monitoring of supported lipid bilayers on various substrates. *Nature Protocols*, 5(6):1096–1106, may 2010.